First-order interface localization-delocalization transition in thin Ising films using Wang-Landau sampling

B. J. Schulz and K. Binder
Institut für Physik, WA331, Johannes Gutenberg Universität, Staudinger Weg 7, D55099 Mainz, Germany

M. Müller
Department of Physics, University of Wisconsin–Madison, 1150 University Avenue, Madison, Wisconsin 53706-1390, USA
(Received 11 October 2004; published 15 April 2005)

Using extensive Monte Carlo simulations, we study the interface localization-delocalization transition of a thin Ising film with antisymmetric competing walls for a set of parameters where the transition is strongly first order. This is achieved by estimating the density of states (DOS) of the model by means of Wang-Landau sampling (WLS) in the space of energy, using both single-spin-flip as well as *N*-fold way updates. From the DOS we calculate canonical averages related to the configurational energy, like the internal energy and the specific heat, as well as the free energy and the entropy. By sampling microcanonical averages during simulations we also compute thermodynamic quantities related to magnetization like the reduced fourth-order cumulant of the order parameter. We estimate the triple temperatures of infinitely large systems for three different film thicknesses via finite size scaling of the positions of the maxima of the specific heat, the minima of the cumulant, and the equal weight criterion for the energy probability distribution. The wetting temperature of the semi-infinite system is computed with help of the Young equation. In the limit of large film thicknesses the triple temperatures are seen to converge toward the wetting temperature of the corresponding semi-infinite Ising model in accordance with standard capillary wave theory. We discuss the slowing down of WLS in energy space as observed for the larger film thicknesses and lateral linear dimensions. In the case of WLS in the space of total magnetization we find evidence that the slowing down is reduced and can be attributed to persisting free energy barriers due to shape transitions.

DOI: 10.1103/PhysRevE.71.046705 PACS number(s): 02.70.Uu, 05.70.Fh, 05.70.Np, 64.60.Cn

I. INTRODUCTION

The restriction of the geometry of a condensed-matter system has fundamental impact on a phase transition. In a finite system, sharp phase transitions can no longer occur, since the free energy is then an analytic function of its independent variables and the transition is rounded off and shifted. A particular realization of a confined geometry in $d=3$ dimensions, playing a pivotal role due to its fundamental importance in material science and technology, are thin films, infinitely extended in two directions but of finite thickness D, where the transition is now not only shifted away from its bulk value, corresponding to $D\to\infty$, but also changes its character from three to two dimensional. As an example we may consider here a fluid near a gas-liquid coexistence in the bulk, or similarly, an (A,B) binary mixture or alloy near phase coexistence, confined between two parallel walls.

Of particular interest is the case where the two walls of the system prefer different phases, i.e., one wall favors high-density liquid (or A particles) while the other one prefers low-density gas (or B particles), which is commonly termed "competing walls." A generic model for such systems actually is the nearest neighbor Ising model in a thin film geometry where one now has two surfaces a distance D apart, on which magnetic surface fields $H_1=-H_D$ of opposite sign but equal magnitude act in order to mimic the competing walls (see Fig. 1). In addition one allows for a different interaction $J_s>0$ between nearest neighbors located in the surfaces, while nearest neighbors in the bulk interact with a coupling $J>0$. The meaning of the magnetic surface fields becomes apparent, when reinterpreting the Ising Hamiltonian as a lattice gas for a fluid or a mixture, where Ising spins $S_i=-1$ or $+1$ now correspond to lattice sites i being empty or occupied, or being taken by an A or a B particle, respectively. Then, surface magnetic fields translate into chemical potentials, i.e., binding energies to the walls.

Remarkably, the transition that one encounters in the Ising film differs from the transition in the bulk system at $T_{\rm cb}$ [1–8]: For all finite thicknesses D of the film, the transition at $T_{\rm cb}$ is completely rounded off and no singular behavior shows up, despite the fact that the system is infinite in the

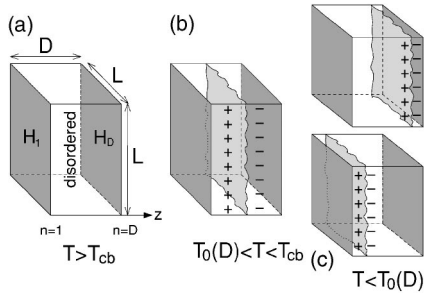

FIG. 1. (a) Thin film geometry with two free surfaces at $n=1$ and D (shaded gray) on which magnetic surface fields H_1 and H_D act. Here, the surface at $n=1$ favors spin up $(+)$, while the surface at $n=D$ favors spin down $(-)$. Parallel to the $L\times L$ surfaces, periodic boundary conditions are imposed. (b) Delocalized interface. (c) Interface located at either of the two surfaces.

other directions. Instead, one observes a transition at a lower temperature $T_0(D) < T_{cb}$, at which the system changes from a state with a delocalized interface running parallel to the walls in the center of the film $[T_0(D) < T < T_{cb}]$, to a twofold degenerate state $[T < T_0(D)]$, where the interface is now localized near one of the two walls (see Fig. 1). Most interestingly, for $D \to \infty$, the transition temperature $T_0(D)$ of the interface localization-delocalization does not converge toward the bulk critical temperature T_{cb}, but toward the wetting temperature $T_w(H_1)$ at which a macroscopically thick liquid layer (spins pointing upward) wets the surface in the corresponding semi-infinite system. Thus, the nature of the transition at finite D is seen to depend on the nature of the wetting transition in the underlying semi-infinite system. Upon enhancing the interaction J_s of spins in the surfaces with respect to the bulk interaction J one can tune the wetting transition and thus the interface transition for finite film thicknesses D to be of first order [8], i.e., $T_0(D) \equiv T_{tr}(D)$ is now a triple point where the three phases shown in Figs. 1(b) and 1(c) coexist. By reducing the film thickness one may then pass through a tricritical point where the order of the transition changes from first to second order [2,8,9].

Our paper is arranged as follows. First, we briefly introduce the thin film Hamiltonian and give a description of the employed Wang-Landau sampling (WLS) which aims at sampling the density of states (DOS) directly. The slowing down of WLS for our model, encountered especially for large system sizes is discussed. With regard to these difficulties we then propose to split the DOS into a branch contributing to the ordered phase and one contributing to the disordered phase, which we normalize separately. We then present the thermodynamic quantities calculated from the DOS and compute the infinite lattice triple temperatures from the various finite size data. Finally, the wetting temperature of the semi-infinite system is determined via the Young equation and the convergence of the triple temperatures towards the wetting temperature for increasing film thickness is examined. We close with a brief discussion of our results.

II. MODEL AND SIMULATION METHOD

We consider the Ising Hamiltonian on a cubic lattice in a $L \times L \times D$ geometry [see Fig. 1(a)], where $N = L^2 D$ is the total number of spins S_i (we measure all lengths in units of the lattice spacing and energy is measured in the same units as the normalized temperature $k_B T$ and, hence, the ratios $J/k_B T$, etc., are all dimensionless):

$$\mathcal{H} = -J \sum_{\langle i,j \rangle_b} S_i S_j - J_s \sum_{\langle i,j \rangle_s} S_i S_j - H \sum_i S_i - H_1 \sum_{i \in \text{surface } 1} S_i - H_D \sum_{i \in \text{surface } D} S_i. \quad (1)$$

Here, the sum $\langle i,j \rangle_b$ runs over all pairs of nearest neighbors where at least one spin is not located in one of the surfaces and the sum $\langle i,j \rangle_s$ runs over all pairs of nearest neighbors with both spins located in one of the two surfaces. In this paper we study three different film thicknesses $D = 6$, 8, 12, and linear lateral dimensions ranging from $L = 16$ to 128 (for the two largest choices of D the minimal L is $L = 32$ and 48, respectively). We restrict ourselves here to antisymmetric surface fields $H_1 = -H_D$ and bulk field $H = 0$. By virtue of the symmetry there is an exact degeneracy of the phases where the interface is bound to either of the surfaces, and the triple point and the phase coexistence below $T_0(D)$ occur at $H = 0$. We do not study prewettinglike phase coexistence for $T > T_0(D)$ and $H \neq 0$. Specifically we choose $H_1/J = 0.25$ and $J_s/J = 1.5$. For these parameters the interface localization-delocalization transition is clearly first order for all thicknesses D. Already for a smaller surface-to-bulk coupling ratio $J_s/J = 1.45$, the transition turned out to be so strongly first order according to the study of Ferrenberg *et al.* [8] that lattices with $D = 8$ and $L > 32$ could not be equilibrated using a standard canonical heat-bath algorithm. The reason for such difficulties can be seen directly from the canonical probability distribution $P_{L,D}(E)$ of the energy which develops two pronounced peaks at the transition point, corresponding to coexisting ordered $(-)$ and disordered phases $(+)$ which are separated by a deep minimum $P_{L,D}^{\min}(E)$ corresponding to the mixed phase configurations (see Fig. 2). Here, one has additional interfaces in the system which cost an extra free energy $\Delta F_{L,D} = \gamma DL$, where γ is of the order of the interface tension between the two oppositely oriented domains of spins. This yields $P_{L,D}^{\min}(E) \propto \exp(-\beta \Delta F_{L,D})$, where $\beta = 1/k_B T$ denotes the inverse temperature. Hence, any simulation technique which aims at sampling a canonical energy probability distribution proportional to $g(E)\exp(-E/k_B T)$ directly will become trapped in the phase in which the system was initially prepared and may practically never escape from there, even in the case of relatively small systems.

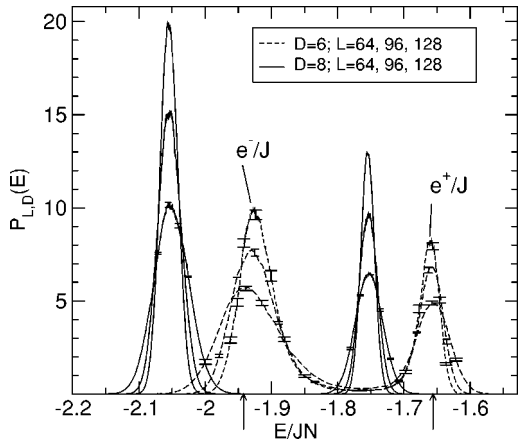

FIG. 2. Energy probability distributions $P_{L,D}$ at equal weight. The peak positions $e^-(L,D)$ and $e^+(L,D)$ (indicated for $D = 6$ and $L = 128$) define the finite volume latent heats $\Delta e(L,D) = e^+(L,D) - e^-(L,D)$. Arrows pointing on the energy axis indicate the interval I_{center}, Eq. (10), in case of $L = 128$ and $D = 6$.

In order to give an example for the strong metastability, Fig. 3 shows hysteresis loops of the internal energy per spin $\langle e \rangle \equiv \langle E \rangle / N$ which were recorded using a conventional Metropolis Monte Carlo algorithm for a system of size $D = 12$ and $L = 48$. The simulations were started in the disordered phase. In case cooling is performed too fast (open circles in

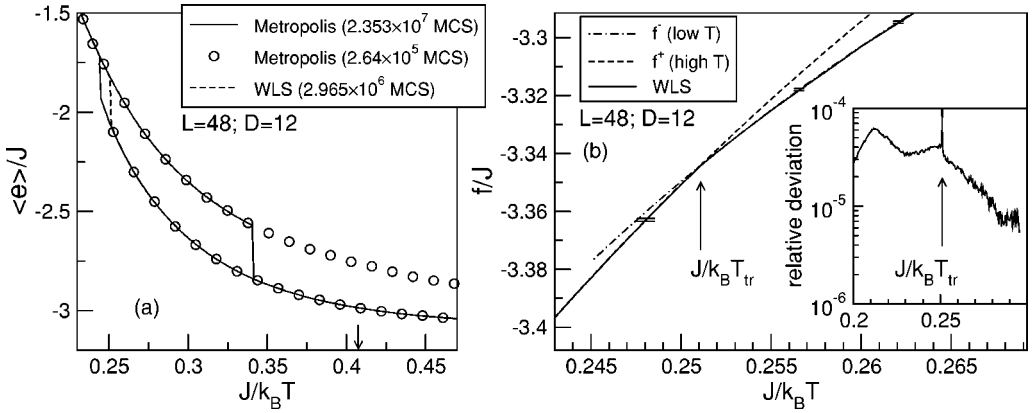

FIG. 3. (a) Energy hysteresis curves. Cooling (heating) was performed at a rate of $J\Delta\beta/\mathrm{perMCS}=4.3403\times10^{-6}$ (open circles, note that not all data points are plotted) and in steps of $J\Delta\beta=0.0005$, using 100 MCS for equilibration at each β and another 10^4 MCS for measuring the energy (solid line). The equilibrium curve obtained from WLS in the space of energy is also shown. The roughening temperature $J/k_BT_R=0.407\,58(1)$ [10] is indicated by an arrow. (b) Low- and high-temperature branches of the free energy per site $f^{\pm}$ as obtained from thermodynamic integration, which yields $J/k_BT_{tr}(D=12)=0.2511(10)$. The relative deviation $|f_{WLS}-f^{\pm}|/f_{WLS}$ between the thermodynamic integration and the WLS result is plotted in the inset.

Fig. 3) one reaches the roughening temperature T_R while still being in the disordered soft-mode phase, i.e., the interface becomes flat in the center of the film and it becomes impossible to reach the ordered phase upon further cooling. Using a much larger simulational effort [$\sim10^7$ Monte Carlo steps (MCS)] one obtains a closed loop—although the observed hysteresis is still huge—which clearly indicates a phase transition in the range $0.244<J\beta_{tr}<0.341$. Locating the exact transition point in this way would however require an enormous simulational effort even for the moderate system size at hand. An improvement results from thermodynamic integration of the low- and high-temperature branches of the internal energy, which yields the free energy per site f [11,12]:

$$\beta f(\beta)=\beta_{\mathrm{ref}}f(\beta_{\mathrm{ref}})+\int_{\beta_{\mathrm{ref}}}^{\beta}\langle e\rangle_{\beta'}d\beta'. \tag{2}$$

For the reference values we have regarded the spins as noninteracting at $J\beta_{ref}=0.000\,05$, i.e., $f(\beta_{ref})=-\beta_{ref}^{-1}\ln 2$, while on the low-temperature side the free energy was matched with a series expansion based on the first two excited states at $J\beta_{ref}=1.100\,05$. The crossing point of both branches of the free energy then yields the transition point, which can be determined with an accuracy of 0.4%.

The result that the correct location of the first-order transition is not in the middle of the hysteresis loop but very close to its end at the high-temperature side (dashed curve in Fig. 3) is very surprising at first sight. It should be noted, however, that the hysteresis observed in Monte Carlo simulations has nothing to do with the "Maxwell equal area rule" of mean field theories, but is of kinetic origin. The almost free interface in the center of the film is very slowly relaxing and feels only a very weak potential from the walls, and thus is much more metastable than the state where the interface is tightly bound to one of the walls.

A. Wang-Landau sampling

To avoid problems due to metastability and to further increase accuracy, we have decided to use Wang-Landau sampling [13–16] in order to compute thermodynamic quantities of the systems via estimating the density of states of Hamiltonian (1). Instead of using the canonical ensemble the Monte Carlo chain generates states with a uniform distribution over a predetermined energy interval. Using reweighting techniques one can subsequently reconstruct canonical averages over a wide range of temperatures. To uniformly sample the energy, one accepts trial configurations with probability $\min[1,g(E)/g(E')]$, where $g(E)$ is the DOS and E and E' are the energies of the current and the proposed configuration, respectively. Since the DOS is not known in the beginning of the simulation, it is set equal to 1 for all energies E. After each spin-flip trial the DOS is modified $g(E)\to g(E)f_i$ by means of a modification factor f_i which is the same for all energies E. For the first stage of the simulation we have chosen the initial value $f_0=e$ in accord with previous studies [13,14] where e is Euler's constant. Periodically one checks if the accumulated energy histogram, $H(E)$, is flat, i.e., $H(E)\geqslant\epsilon\langle H(E')\rangle_{E'}$ for all E. These checks were performed after 10^2–10^3 Monte Carlo sweeps. If the histogram is flat, the modification factor is reduced according to $f_{i+1}=\sqrt{f_i}$ and the histogram of visited states, $H(E)$, is then reset to zero and the procedure is repeated until a flat $H(E)$ is achieved using a final modification factor f_{final}. The latter value is typically on the order between $1.0+10^{-9}$ and $1.0+10^{-6}$. Thus, starting with the above choice for f_0, the WLS passes through a sequence of at least 20 iterations before the final stage using f_{final} is performed. In practice one samples a logarithm of the DOS, i.e., $\log_{10}g(E)$, since $g(E)$ may become very large and modifying the DOS then corresponds to adding a small modification increment $\Delta s_i=\log_{10}f_i$. The implementation of the single-spin-flip WLS is straightforward and we refer the reader to Refs. [13–15] for details. When considering systems with a large number of distinct energy levels it is useful

to partition the entire energy range into adjacent subintervals in order to sample the DOS in a parallel fashion. For energy intervals that contain states with low degeneracy, e.g., the ground state, one can further accelerate WLS by combining it with the rejection-free N-fold way of Bortz *et al.* [16,17]. Here, the underlying idea is to partition all spins S_ν, $\nu \in \{1,\ldots,N\}$, into M classes $c_\nu \in \{0,\ldots,M-1\}$ according to the change in energy ΔE_{c_ν} caused by flipping a spin S_ν at site ν. Making explicit use of $H_1 = -H_D$ and $H=0$ in the Ising Hamiltonian (1), we can evaluate ΔE_{c_ν} as follows:

$$\Delta E_{c_\nu} = \begin{cases} 2(Ju_\nu + J_s v_\nu + H_1)S_\nu & \text{if } \nu \in \text{surface } 1, \\ 2(Ju_\nu + J_s v_\nu - H_1)S_\nu & \text{if } \nu \in \text{surface } D, \\ 2Ju_\nu S_\nu & \text{else}, \end{cases} \tag{3}$$

where S_ν is the spin value before it is overturned and u_ν and v_ν denote sums over the nearest neighbor sites $\mu(\nu)$ of site ν:

$$u_\nu = \begin{cases} \sum_{\mu(\nu)} S_{\mu(\nu)} & \text{if } \nu \notin \text{surface}, \\ \sum_{\mu(\nu) \notin \text{surface}} S_{\mu(\nu)} & \text{if } \nu \in \text{surface}, \end{cases} \tag{4}$$

and

$$v_\nu = \begin{cases} 0 & \text{if } \nu \notin \text{surface}, \\ \sum_{\mu(\nu) \in \text{surface}} S_\mu & \text{if } \nu \in \text{surface}. \end{cases} \tag{5}$$

This results in a number of $M=27$ different classes. Within the context of the N-fold way WLS the probability of any spin of a class i being overturned is then given by

$$P(\Delta E_i) = \frac{n(\mathcal{C}, \Delta E_i)}{N} p_{\mathcal{C}\to\mathcal{C}'}, \quad i = 1,\ldots,M, \tag{6}$$

where $n(\mathcal{C}, \Delta E_i)$ denotes the number of spins of configuration $\mathcal{C}$ which belong to class i and $p_{\mathcal{C}\to\mathcal{C}'}$ is given by

$$p_{\mathcal{C}\to\mathcal{C}'} = \begin{cases} \min\left(1, \frac{g(E_\mathcal{C})}{g(E_{\mathcal{C}'})}\right) & \text{if } E_{\mathcal{C}'} \in I_{\text{sub}}, \\ 0 & \text{if } E_{\mathcal{C}'} \notin I_{\text{sub}}, \end{cases} \tag{7}$$

where I_{sub} denotes the considered energy subinterval over which the DOS is sampled and $E_{\mathcal{C}'} = E_\mathcal{C} + \Delta E_i$. Classes are now chosen as follows. First, one computes the integrated probabilities for a spin flip within the first m classes:

$$Q_m = \sum_{i \le m} P(\Delta E_i), \quad m = 1,\ldots,M \text{ and } Q_0 = 0. \tag{8}$$

By generating a random number $0 < r < Q_M$ one then finds the class m from which to flip a spin via the condition $Q_{m-1} < r < Q_m$. The spin to be overturned is chosen from this class with equal probabilities, whereby $\log_{10} g(E)$ and the energy histogram are now updated by means of the average lifetime $\tau = 1/Q_M$. A detailed description of the algorithm was given in Ref. [16].

B. Normalization of the DOS

In order to estimate the DOS using WLS, the considered energy range

$$E/JN \in I = [E_{\text{ground}}/JN, 0.2], \tag{9}$$

where $E_{\text{ground}} = -[(3D-5)J + 4J_s]N/D$, is the twofold degenerate ground state energy, was partitioned into several adjacent subintervals each containing an order of 10^2 to 10^3 distinct energy levels, which were sampled on a Cray T3E in a parallel fashion using mostly 64 processors at a time. The DOS obtained from these simulations was then matched at the edges and suitably normalized, which we will describe in detail below. For the system thicknesses $D=8$ and 12, as well as for the largest choices of L in the case of $D=6$ ($L=96$, 128) only one run was performed over the entire energy range (9) denoted as the basis run, whereas all further runs have been restricted to a smaller energy range

$$E/JN \in I_{\text{center}} = [E_1/JN, E_2/JN], \tag{10}$$

covering the mixed phase region in between the peaks of the doubly peaked energy distribution. As an illustration, I_{center} is marked in Fig. 2 by small arrows on the energy axis. Thus, the entire energy range (9) is decomposed as $I = I_{\text{left}} \cup I_{\text{center}} \cup I_{\text{right}}$, where we have $I_{\text{left}} = [E_{\text{ground}}/JN, E_1/JN]$ and $I_{\text{right}} = [E_2/JN, 0.2]$. Correspondingly, one obtains the density of states $g(E)$ by joining $g(E)$ estimated for the intervals I_{left} (taken from the basis run), I_{center}, and I_{right} (again taken from basis run).

The single-spin-flip algorithm is more efficient in the regions covered by I_{center} which is due to the added expense of the N-fold way algorithm concerning the bookkeeping of classes. This was affirmed by a rough comparison between both implementations for $L=128$ and $D=12$. The flatness parameter ϵ varied between 0.8 and 0.95, and the final modification increment was usually of order $\Delta s_{\text{final}} \sim 10^{-9}$ which yielded an overall simulational effort of order 10^6–10^7 MCS for estimating the DOS over the range (9). As is clear from the algorithm, WLS only yields a relative density of states; hence available reference values must be employed in order to get the absolute DOS $g(E)$. Normalizing the simulational outcome first with respect to the twofold degeneracy of the ground state, i.e., the free energy f will be exact for $\beta \to \infty$, it is instructive to examine how this accuracy for low temperatures carries over to infinite temperature ($\beta \to 0$), where the partition function Z is dominated by the density of states around $E=0$, and one has $\lim_{\beta\to 0} \beta F(\beta)/N = -(1/N)\ln Z(\beta = 0) = -\ln 2$. Table I shows the latter quantity for all considered system sizes. As can be seen from the table there is an increasing deviation from the exact value with increasing width of the film D. While the results for $D=6$ and 8 (the latter for small sizes L) agree with the expected value, a deviation for the larger system sizes, especially $L=128$ and $D=12$, becomes apparent. This is related to a slowing down in the equilibration process in the multicanonical (Wang-Landau) ensemble for decreasing modification increment Δs_i, as illustrated in Fig. 4 for $L=32$ and $D=8$, which shows the visited states $(E/JN, M/N)$ and the energy histogram $H(E)$ recorded during Wang-Landau sampling for different stages i of the simulation, where the modification increment Δs_i is used to modify the density of states. In case one has a small number of tunneling events during a certain simulation stage i, $H(E)$ exhibits a kink at the barrier, since the stage is

TABLE I. Logarithm of the partition function $-(1/N)\ln Z_{\beta=0}$ of a thin Ising film for different linear dimensions L and D, in case the density of states is normalized with respect to the ground state. The value in parentheses states the standard deviation. The exact value and the deviations from the latter are listed in the last two columns, respectively. For $L=32$ and $D=8$ the run showing the largest deviation from the exact value $[-(1/N)\ln Z_{\beta=0}=-0.692\,624]$ was excluded from data analysis. Then one has $-(1/N)\ln Z_{\beta=0}=-0.693\,07(9)$. Under "No. of runs" we have listed the number of independent simulations.

D	L	No. of runs	$-\frac{\ln Z_{\beta=0}}{N}$	$-\frac{\ln Z^{\text{exact}}_{\beta=0}}{N}$	$\frac{\lvert\ln Z_{\beta=0}-\ln Z^{\text{exact}}_{\beta=0}\rvert}{\lvert\ln Z^{\text{exact}}_{\beta=0}\rvert}$
6	16	6	−0.6932(5)	−0.693147	0.0076%
6	24	3	−0.6931(4)	−0.693147	0.0061%
6	32	3	−0.6932(3)	−0.693147	0.0082%
6	48	3	−0.69318(5)	−0.693147	0.0048%
6	64	5	−0.69311(6)	−0.693147	0.0049%
6	96	2	−0.693112(2)	−0.693147	0.0051%
6	128	6	−0.693144(9)	−0.693147	0.00042%
8	32	4	−0.6930(2)	−0.693147	0.027%
8	48	2	−0.69310(4)	−0.693147	0.0075%
8	64	3	−0.69312(6)	−0.693147	0.0038%
8	96	1	−0.69301	−0.693147	0.020%
8	128	1	−0.69304	−0.693147	0.016%
12	48	3	−0.69240(2)	−0.693147	0.107%
12	64	1	−0.692544	−0.693147	0.087%
12	96	2	−0.692686(3)	−0.693147	0.067%
12	128	10	−0.69281(4)	−0.693147	0.048%

completed once the flatness criterion is satisfied. Correspondingly, $g(E)$ will suffer from large errors in the ordered phase, in case it is normalized using a reference in the disordered phase, and vice versa, errors will be enhanced in the disordered phase when using a reference in the ordered phase (ground state).

For $D=8$ (excluding $L=32$) and $D=12$ we therefore employed the following approach. Utilizing the fact that one has at least random walk behavior for small modification factor in each of the phases alone, we normalize the branch of the density of states $g_-(E)$ contributing to the low-energy ordered phase and the branch $g_+(E)$ contributing to the high-energy disordered phase separately, i.e., one has

$$g(E)=\begin{cases} g_-(E) & \text{for } E\leqslant E_{\text{cut}}, \\ g_+(E) & \text{for } E>E_{\text{cut}}, \end{cases} \tag{11}$$

where one obtains $g_-(E)$ by normalizing the simulational outcome $g(E)$ with respect to the ground state $g(E_{\text{ground}})=2$ and $g_+(E)$ obtained by normalizing $g(E)$ with respect to the total number of states

$$\sum_E g(E)=2^{L^2D}. \tag{12}$$

In Eq. (11), E_{cut} is taken to be the energy for which the energy probability distribution, estimated directly from the simulational outcome $g(E)$, takes its minimum in between the peaks at equal weight. Note that in the sum $\Sigma_E g(E)=\Sigma_{E\leqslant E_{\text{cut}}} g_-(E)+\Sigma_{E>E_{\text{cut}}} g_+(E)$ the term $\Sigma_{E\leqslant E_{\text{cut}}} g_-(E)$ is negligible.

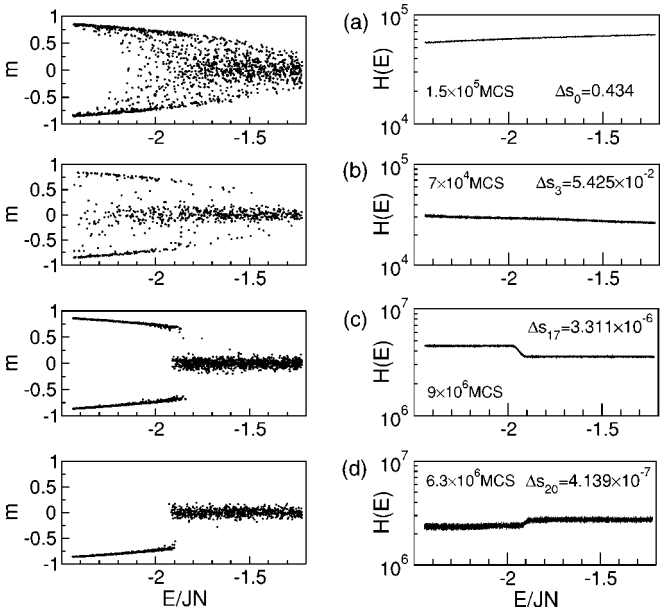

FIG. 4. Visited states $(E/JN, M/N)$ (left hand side) and energy histogram $H(E)$ (right hand side), recorded during WLS in the space of energy over the interval $E/JN\in[-2.4414,-1.2207]$ for different stages i of the simulation. The system size is $L=32$ and $D=8$. The simulation used 3.844×10^7 MCS in total, with a flatness criterion for the energy histogram of $\epsilon=0.9$ and a final modification increment of $\Delta s_{\text{final}}\approx 4.139\times10^{-7}$.

The additional error that is introduced by this normalization procedure then depends on the contribution of the mixed phase configurations to the energy distribution (and the choice of E_{cut}). However, since these mixed phase configurations are exponentially suppressed at the transition point, the error is expected to be also exponentially small, and concomitant error due to the choice of E_{cut} as well. Note that already for $L=32$ and $D=8$ the double Gaussian approximation to the energy probability distribution, which neglects any mixed phase contribution, provides a reasonably good approximation to the measured distribution, apart from small deviations in the tails (see Fig. 5).

C. Shape transitions

In Ref. [18], Neuhaus and Hager addressed the severe problem of slowing down in simulations of first-order transitions in the multicanonical ensemble [19]. This was exemplified by studying the two-dimensional Ising model on $L\times L$ square lattices (periodic boundary conditions) below the critical bulk temperature on the whole magnetization interval $[-L^2,L^2]$ whereby the sampling of configurations with magnetization $M=\Sigma_i S_i$ was biased with the inverse probability distribution of the magnetization $g^{-1}(M)$. Specifically, it was found in Ref. [18] that these simulations suffered from a slowing down due to a discontinuous droplet-to-strip transi-

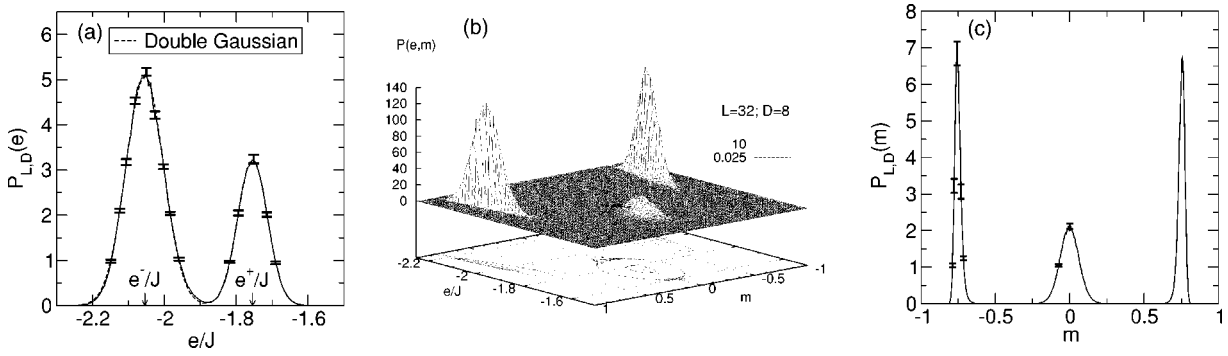

FIG. 5. (a) shows the double Gaussian approximation (25) to the energy probability distribution $P_{L,D}(e)$ for the system of size $L=32$ and $D=8$ at the finite volume transition point $[\beta_{\mathrm{tr}}(L,D)=0.247\,255(10)]$ as obtained from WLS in the space of magnetization (single spin flip) by reweighting back to the canonical ensemble. (b) shows the corresponding full joint energy–order parameter distribution $P_{L,D}(e,m)$. Contour lines for $P(e,m)=10$ and 0.025 are drawn in the e-m plane. (c) shows the projection onto the magnetization axis.

tion [20], i.e., $\tau \propto \exp(2R\sigma L)$, where τ is the tunneling time between droplet and strip configurations, σ is the interfacial tension, and R was measured to be $R=0.121(14)$. Note that one has $R \approx 1$ for nonmulticanonical simulations.

Of course, one needs a fairly good approximation to $g(M)$, in order to sample the considered Hamiltonian in the multicanonical ensemble. Within the framework of WLS one may therefore simulate the system at a certain inverse temperature β of interest by employing the flipping probability (single-spin-flip Metropolis)

$$p_{\mathcal{C}\to\mathcal{C}'} = \min\left[1, \frac{g(M_{\mathcal{C}})}{g(M_{\mathcal{C}'})}\exp(-\beta[E_{\mathcal{C}'} - E_{\mathcal{C}}])\right], \qquad (13)$$

for the transition from the state $\mathcal{C}$ to the state $\mathcal{C}'$. Each time a state with magnetization M is visited, one updates $g(M)$ according to $g(M)\to g(M)f_i$ in complete analogy to the case where $g(E)$ is used. Once this procedure has rendered $g(M)$ accurate enough, one makes a production run, where $g(M)$ is not altered anymore. Thermodynamic quantities can then be obtained by reweighting to the canonical ensemble.

For the first-order interface transitions in thin Ising films as studied here, we have found evidence that geometrical transitions in the ensemble realized by Wang-Landau sampling in the space of magnetization indeed hamper the simulations. While this poses no problem for the smaller systems like $D=8$ and $L=32$ where WLS using $g(M)$ yields very good results (see Fig. 5), we observe pronounced effects for the largest considered system size. This is shown in Fig. 6(b) where part of a time series is depicted which was recorded for $D=12$ and $L=128$ during WLS in the space of total magnetization. The simulation was restricted to the interval $m=M/N\in[-0.559\,49,-0.457\,76]$ after monitoring the time series of m for a much larger interval $m\in[-0.915\,53,0.101\,73]$ where Δs_i decreased from 5.0×10^{-3} to 7.629×10^{-8} over a simulation time of 1.632×10^7 MCS at $J/k_{\mathrm{B}}T=0.2497\,19$. The distribution $g(M)$ was then further iterated on the interval $m\in[-0.559\,49, -0.457\,76]$ where Δs_i was refined from 1.0×10^{-5} to 1.953×10^{-8} within 7.27×10^6 MCS and finally held fixed such that the depicted time series could be recorded. Configurations were thereby monitored along the estimated position of the barrier $m\approx -103\,000/N=-0.523\,885$. Figures 6(a) and

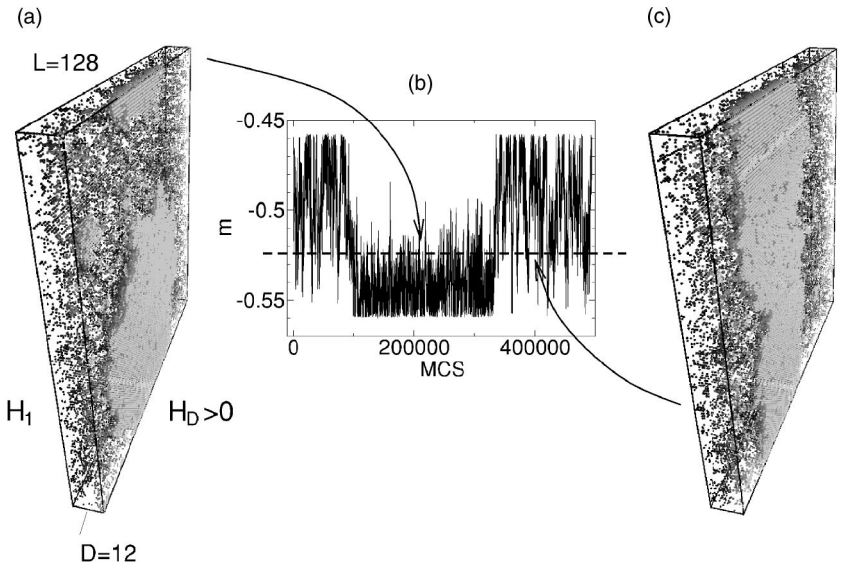

FIG. 6. (a) Droplet at surface $n=D$ where the positive field $H_D/J=0.25$ acts. (b) Selected part of a time series of the total magnetization per spin $m=M/N$ as produced by WLS (single-spin-flip) in the space of magnetization. (c) Percolated striplike droplet. Note that in (a) and (c) only the positive spins are displayed as small spheres. Those spins closest to the shown $L\times L$ surface are the lightest.

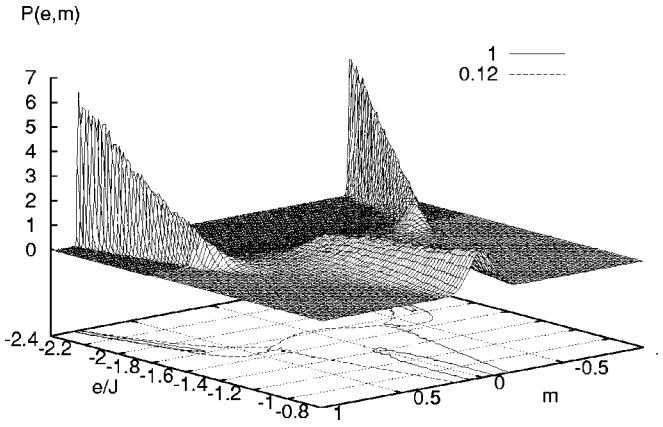

FIG. 7. Joint energy–order parameter distribution $P(e,m)$ as obtained from WLS in the space of energy for a system size of $D=6$ and $L=16$. Contour lines for $P(e,m)=1$ and 0.12 are drawn in the e-m plane. The distribution was recorded using a fixed DOS $g(E)$, which was taken from the usual adaptive WLS.

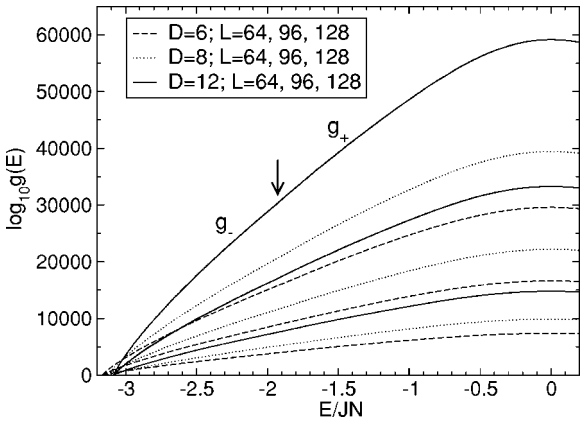

FIG. 8. Logarithm of the energy density of states $\log_{10}[g(E)]$ for thicknesses $D=6,8,12$ and linear dimensions $L=64,96,128$. Smaller choices for L (in case of $D=6$ and 8) are omitted in order to preserve clarity. Also indicated by an arrow is the region where E_{cut}, appearing in Eq. (11), is typically located. Here, both branches of the density of states g_- and g_+, are joined ($D=8,12$). In the case of $D=6$, $g(E)$ was normalized solely with respect to the ground state degeneracy.

6(c) show snapshots of the two possible coexisting structures which are the three-dimensional analogs (in the presence of a surface) to the droplet and strip shapes as studied in Ref. [18]. In case Wang-Landau sampling is performed in the energy space, the governing mechanism of the slowing down is not determined up to now. From the joint energy–order parameter distribution (Fig. 7), however, recorded for Wang-Landau sampling in the space of energy, one can at least conclude that one suffers from the fact that the ordered and the disordered phases are not distinctly separated in energy, as can be seen by inspecting the distribution of magnetization (along lines of constant energy) which shows a noticeable three-peak structure around energies $e/J \approx -1.7$. Thus, the WLS using $g(E)$ does not remove the barriers between the ordered and disordered states. These barriers are much larger than the barrier encounter during the WLS using $g(M)$ (due to shape transitions) and result in a severe slowing down of the WLS using $g(E)$ compared to WLS using $g(M)$. Further studies are clearly necessary in order to clarify whether there are connections to droplet related phenomena.

III. SIMULATION RESULTS

A. Thermodynamic quantities

From the simulated DOS, as depicted in Fig. 8, we have calculated the first and second moments of the energy per spin

$$\langle e^n \rangle = \frac{1}{N^n Z(\beta)} \sum_E E^n g(E) \exp(-\beta E), \tag{14}$$

and the specific heat

$$c = \frac{N}{k_B T^2} (\langle e^2 \rangle - \langle e \rangle^2). \tag{15}$$

Furthermore, important quantities like the free energy per spin can be directly computed,

$$f = -\frac{1}{N\beta} \ln Z(\beta) = -\frac{1}{N\beta} \ln \left[\sum_E g(E) e^{-\beta E} \right], \tag{16}$$

and the entropy per spin can be obtained from the internal energy (14) and the free energy (16),

$$s = \frac{\langle e \rangle - f}{T}. \tag{17}$$

By measuring microcanonical averages $\langle \cdot \rangle_E$ during the last stage of a one-dimensional random walk in energy space, where $g(E)$ is updated with the smallest increment $\Delta s_{\mathrm{final}}$ we can also compute canonical averages of the order parameter (and higher moments)

$$|m| = \frac{1}{N} |M| = \frac{1}{N} \left| \sum_{i=1}^{N} S_i \right|, \tag{18}$$

i.e.,

$$\langle |m|^n \rangle = \frac{\sum_E \langle |m|^n \rangle_E g(E) e^{-\beta E}}{\sum_E g(E) e^{-\beta E}}. \tag{19}$$

Thus quantities like the finite lattice susceptibility χ

$$\chi = \frac{N}{k_B T} (\langle m^2 \rangle - \langle |m| \rangle^2), \tag{20}$$

as well as the fourth-order cumulant U_4 on which we concentrate in the following and which is defined as

$$U_4 = 1 - \frac{\langle m^4 \rangle}{3 \langle m^2 \rangle^2}, \tag{21}$$

become accessible.

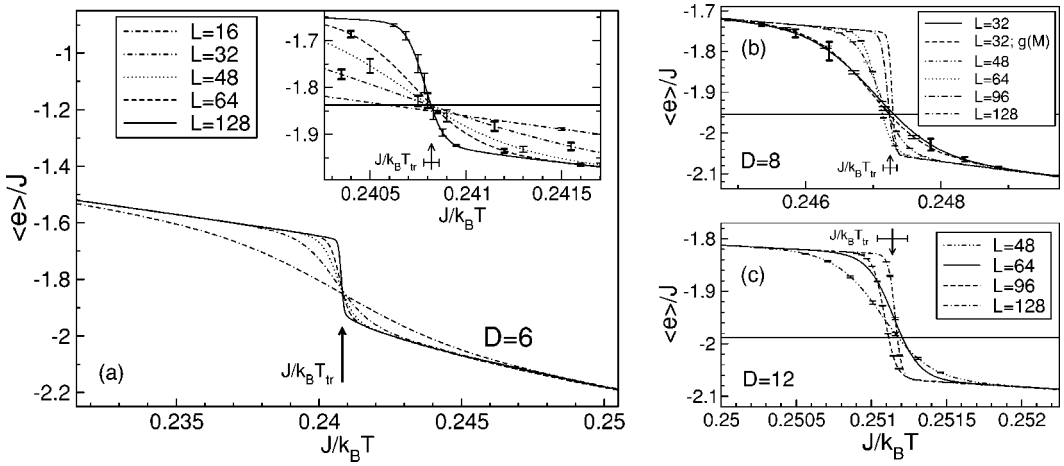

FIG. 9. Internal energy $\langle e\rangle$ for different linear dimensions L and film thicknesses D. Lines are obtained from reweighting the results of the WLS. Estimates for the inverse temperature $J\beta_{\mathrm{tr}}(D)=J/k_{\mathrm{B}}T_{\mathrm{tr}}(D)$ of the triple point are indicated by arrows. The horizontal solid lines mark the value $(e^{+}+2e^{-})/3$ where the curves are expected to cross. In (b) the data obtained from WLS using $g(M)$ ($D=8$ and $L=32$) are plotted for comparison. Here, $g(E)$ for $D=8$ and $L=32$ was normalized solely with respect to the ground state. Within the inverse temperature range displayed in the inset of (a), the average relative errors in $\langle e\rangle$ for $D=6$ amount to 0.17%, 0.54%, 0.55%, 0.42%, and 0.45% for $L=16,\ldots,128$, respectively. For $D=8$ and $L=32$ the average error amounts to 0.18% in the range $0.2455\leqslant J/k_{\mathrm{B}}T\leqslant 0.2485$, when using $g(M)$ while it is 1.0% within the same range when using $g(E)$. Note that for $D=8$ and $L=96,128$, as well as for $D=12$ and $L=64$ the DOS was determined only once; hence no error bars are displayed.

The distinctive feature of first-order phase transitions are phase coexistence and metastability. For the interface localization-delocalization transition considered here, this is reflected by jump discontinuities in the internal energy $\langle e\rangle$ as well as the (absolute) magnetization $\langle|m|\rangle$ per site, which are depicted in Figs. 9 and 10, respectively, and also by hysteresis effects encountered when heating and cooling the system as exemplified in Fig. 3. Considering the internal energy (Fig. 9) for fixed D and varying linear dimension L, one can clearly see that one actually does not observe discontinuous jumps of the quantities in question but a continuous behavior that sharpens to the asserted steplike behavior with increasing linear system size L. This rounding is related to the fact that a true phase transition can only occur in the thermodynamic limit, where in equilibrium, approaching the transition temperature from above, the energy of the system discontinuously jumps from e^{+} (interface in the center of the film) to e^{-} (interface tightly bound to the wall), while for a finite volume the system may jump back and forth between the latter states and the observed equilibrium behavior is thus continuous in temperature. The rounding of the transition in finite systems can also be observed for the specific heat c depicted in Fig. 11 which exhibits narrow peaks that are remnants of the δ-function singularities one would get when differentiating the discontinuous energy in the infinite volume limit. Apart from the finite size rounding, one can see that the positions of the maxima of c and the minimum of the fourth-order cumulant U_4 (Fig. 12) are systematically shifted towards higher β values for increasing linear dimension L.

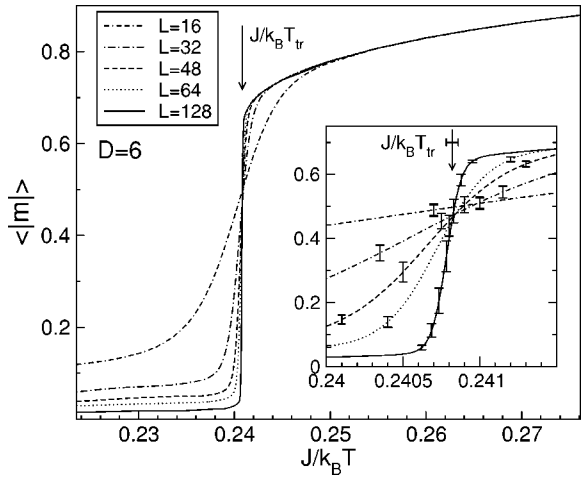

FIG. 10. Average absolute magnetization per spin $\langle|m|\rangle$ of a thin Ising film for different linear dimensions L and film thicknesses D. Within the inverse temperature range displayed in the inset of (a), the average relative errors in $\langle|m|\rangle$ for $D=6$ amount to 1.0%, 5.2%, 6.3%, 6.1%, and 9.3% for $L=16,\ldots,128$, respectively.

From the crossings of the energy curves for different linear dimensions L, one can get a first idea about the achieved accuracy for the different film thicknesses D, because they should cross to a very good approximation in the point [21]

$$(\beta_{\mathrm{tr}}(D),(e^{+}+2e^{-})/3), \tag{22}$$

where $\beta_{\mathrm{tr}}(D)$ is the infinite system transition point. Hence, the crossing points for different L,

$$\langle e(\beta_{\mathrm{cross}},L,D)\rangle=\langle e(\beta_{\mathrm{cross}},L',D)\rangle, \tag{23}$$

actually provide an estimator for the infinite system transition temperature, which is expected to deviate from $\beta_{\mathrm{tr}}(D)$ only by an amount exponentially small in system size [21]. As can be seen from the inset of Fig. 9(a) in the case of $D=6$, the various crossings are indeed scattered in a narrow region around the extrapolated infinite volume transition point for $L\geqslant 32$. For smaller values of L exponential correc-

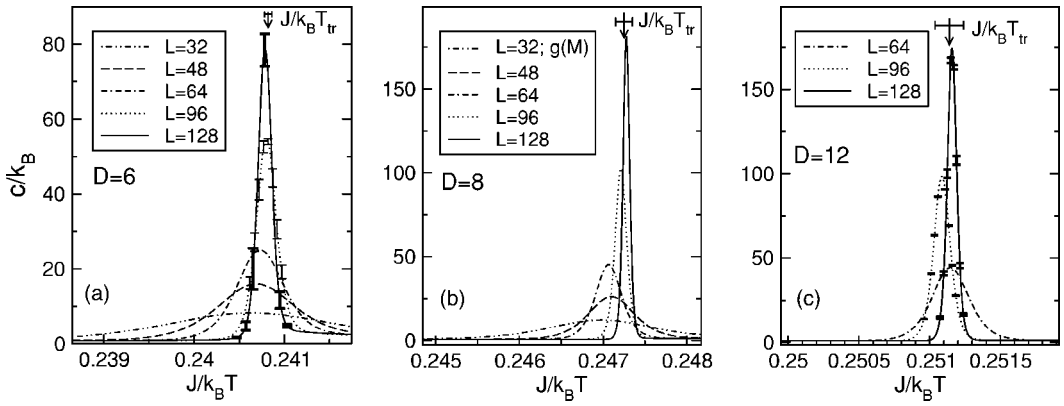

FIG. 11. Specific heat c of a thin Ising film for different linear dimensions L and film thicknesses D. In the interval $0.2400 \leqslant J/k_BT \leqslant 0.2415$ the average relative error for $D=6$ amounts to 3.9%, 9.6%, 12.0%, 5.4%, and 15.9% for $L=32,\ldots,128$, respectively. For $D=8$ and $L=32$, Wang-Landau sampling in $g(M)$ yields an average error of 2.6% within the range $0.2455 \leqslant J/k_BT \leqslant 0.2480$. Note that we have no statistics for $D=8$ and $L=96,128$ (b), as well as for $D=12$ in case of $L=64$ (c).

tions still make a noticeable contribution. For the larger thicknesses $D \geqslant 8$ the region where the energy curves cross is noticeably larger. Particularly, one obtains that the errors resulting from averaging over different runs are too small to fully account for the deviations [excluding $L=32$ for which $g(M)$ was employed]. This is related to the fact that for the thicknesses $D=8$ and 12 only a single run was performed over the entire energy range (9) while further runs were restricted to the mixed phase region in between the peaks, because the slowing down, as described in the preceding subsection, was not foreseen. When one uses the normalization condition (11), the proper strategy would certainly be to enhance the simulational effort in the pure phases, down to the ground state and up to $E=0$, since the reference density of states is known for $T=0$ and $\beta=0$. This is necessary, in order to minimize the accumulation of errors in the density of states, since the Wang-Landau method and similar adaptive algorithms, do not in general exhibit an error distribution that is flat in energy. [1] Hence, for $D=8$ [excluding the simulation using $g(M)$] and $D=12$, we believe the true errors to be larger than the error bars displayed in Figs. 9(b), 9(c), 12(b), 11(b), and 11(c) and when quantitatively referring to errors of the thermodynamic quantities, we thus restrict ourselves here to $D=6$, where we have reliable error estimates for $L=16$, 24, 32, 48, and 64.

Exponential corrections to the crossing points are presumably much smaller than the scatter in the energy crossings for $D \geqslant 8$ and one may therefore conclude that the deviations in the crossings for $D \geqslant 8$ are not due to corrections to scaling, but reveal the actual error in the density of states for this region. This is also the case for the other quantities like the

[1] Recently, an adaptive algorithm was proposed [35] which aims at maximizing the number of round trips between both edges of an energy interval which has the additional benefit of exhibiting a flat error distribution.

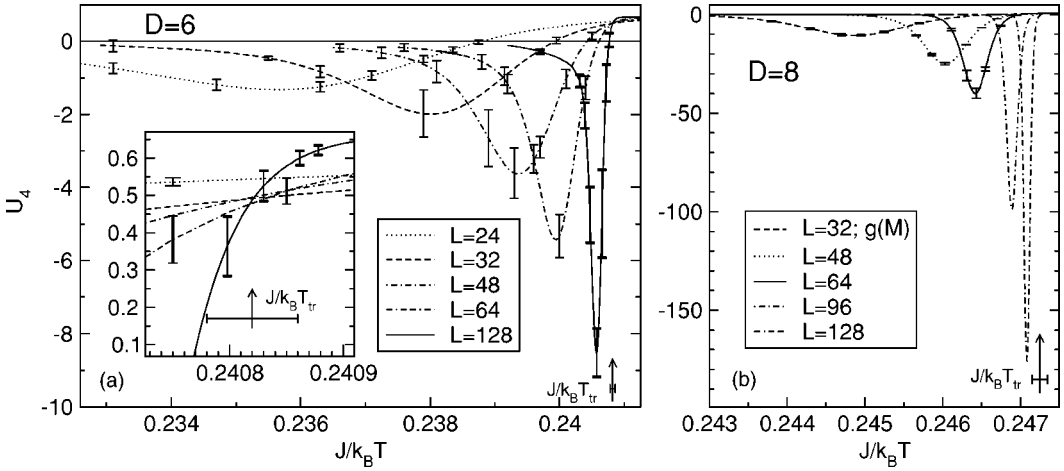

FIG. 12. Reduced fourth-order cumulant of a thin Ising film for different linear dimensions L and film thicknesses D. The inset of (a) shows the region where the cumulants for the various linear sizes L cross ($D=6$). In the vicinity of the minima positions, the relative errors in U_4 in the case of $D=6$ amount to 11%, 30%, 17%, 11%, and 7% for $L=24,\ldots,128$, respectively. WLS in the space of total magnetization M with fixed $g(M)$ yields an error of 4% ($D=8, L=12$). Note that for the data corresponding to $D=8$, as plotted in (b), we have no statistics for $L=96$ and $L=128$, i.e., for the latter sizes the DOS was estimated only once.

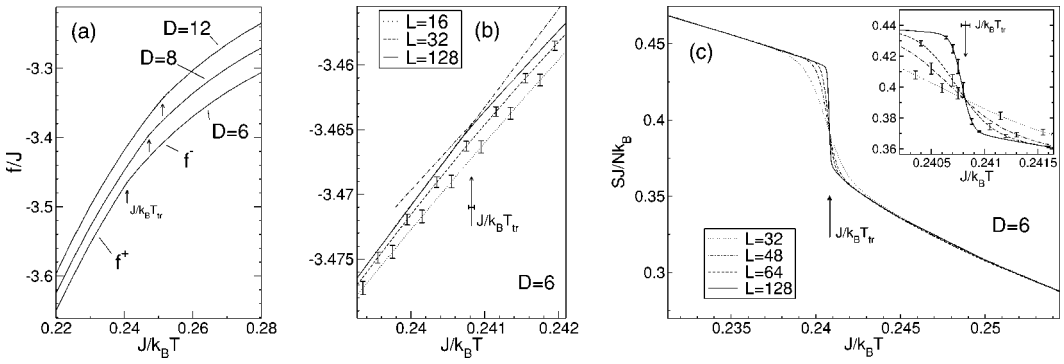

FIG. 13. (a) Free energy per spin f of a thin Ising film for different linear dimensions L and film thicknesses D. Note that in (a) only the data for $L=128$ are plotted, while (b) shows f on a finer scale. In the range $0.23 \leqslant J/k_B T \leqslant 0.27$, the average relative error in the free energy ($D=6$) is 0.0143%, 0.011%, and 0.000 26% for $L=16$, 32, and 128, respectively. (c) Entropy per spin s for $D=6$. The error in s amounts to 0.64%, 0.64%, 0.47%, and 0.47%, within the range depicted in the inset of (c).

specific heat for example [Figs. 11(b) and 11(c)]. Thus, the analysis of the systems with larger thicknesses $D=8$ and 12 is certainly more difficult and less accurate.

One can however roughly estimate the order of magnitude of the latter uncontrolled error, which also serves to support the above picture. For example, from the density of states of the largest system ($D=12$ and $L=128$), one can estimate that a relative error in the density of states $g(E)$ of the order $\sim 10^{-1}$ [referring to the results for the 50×50 two-dimensional (2D) Ising model in Ref. [16] this seems to be a reasonable assumption], in the narrow region corresponding to the peak of the ordered phase of the energy probability distribution, can result in a displacement $\Delta\beta$ of the peak position $\beta_{c\max}$ of the specific heat and also of the step location of the internal energy, which is approximately of the order $\Delta\beta/\beta_{c\max} \sim 10^{-4}$. In the case of $D=12$ and $L=48$, a relative deviation of this order could already be caused by a relative error in $g(E)$ which is of the order $\sim 10^{-2}$ in the above region. These considerations comply well with the observed scatter.

B. Finite size scaling

When one deals with second-order phase transitions, the characteristic feature is a divergent spatial correlation length ξ at the transition point β_c (where one observes fluctuations on all length scales) implying power-law singularities in thermodynamic functions such as the correlation length, magnetization, specific heat and susceptibility. This is in sharp contrast to a first-order transition where the correlation length in the coexisting pure phases remains finite and concerning finite size scaling the volume of the system turns out to be the relevant quantity. For a thin film geometry where one has fixed D and varying linear dimension L, finite size scaling will thus involve the quantity L^2. This can be shown by approximating the energy distribution $P_{L,D}(e)$ of the pure phases by a Gaussian [21–23] centered around the infinite-lattice energy per spin $\langle e\rangle$

$$P_{L,D}(e) = \sqrt{\frac{L^2 D}{2\pi k_B T^2 c}} \exp\left[\frac{(e-\langle e\rangle)^2}{2k_B T^2 c} L^2 D\right], \qquad (24)$$

where c denotes the infinite-lattice specific heat. Since one has phase coexistence at a first-order transition, the probability distribution of the energy will be double peaked at the transition point $\beta_{tr}(D)=1/k_B T_{tr}(D)$, where $\langle e\rangle$ jumps from e^- (low-energy phases, interface at one of the two walls) to e^+ (single high-energy phase, interface centered in the middle of the film), i.e., the free energy branches $f^\pm$ intersect at a finite angle in the infinite system, as can be seen from Fig. 13(a), when inspecting the curves around the transition point [cf. also Fig. 3(b)] It is essentially this nonanalyticity in the free energy, which gives rise to the discontinuous behavior of the internal energy. In a finite system however, the free energy remains differentiable and the intersection is rounded.

Hence, at the transition point, $P_{L,D}(e)$ is a superposition of two Gaussians (24) centered at $\langle e\rangle = e^\pm$, while slightly away from the transition at $T=T_{tr}+\Delta T$ they are centered at energies $e^\pm + c^\pm \Delta T$, where $c^\pm$ are the specific heats in the disordered (+) and ordered phases (−), which are assumed to be constant in the vicinity of the transition, i.e., for sufficiently small ΔT. Each of the Gaussians is then weighted by Boltzmann factors of the corresponding free energies $f^\pm$, and one thus arrives at

$$P_{L,D}(e) = A\left\{\frac{a^+}{\sqrt{c^+}}\exp\left[-\frac{[e-(e^+ + c^+\Delta T)]^2}{2k_B T^2 c^+} L^2 D\right] + \frac{a^-}{\sqrt{c^-}}\exp\left[-\frac{[e-(e^- + c^-\Delta T)]^2}{2k_B T^2 c^-} L^2 D\right]\right\}, \qquad (25)$$

where the weights $a^\pm$ are given by

$$a^\pm = q^\pm \exp\left[\mp \frac{f^+ - f^-}{2k_B T} L^2 D\right], \qquad (26)$$

and A reads

$$A = \exp\left[-\frac{(f^+ + f^-)}{2k_B T} L^2 D\right] \sqrt{\frac{L^2 D}{2\pi k_B T^2}}. \qquad (27)$$

Since we have a single high-energy phase and two low-energy ordered phases we set $q^+=1$ and $q^- \equiv q=2$ in the following. At the transition all phases have equal weight [21,24] such that the area under the peak at e^- is q times the area under the peak at e^+ which is satisfied by Eq. (25). Within the framework of the ansatz (25) one then proceeds by calculating the energy moments as usual via [22]

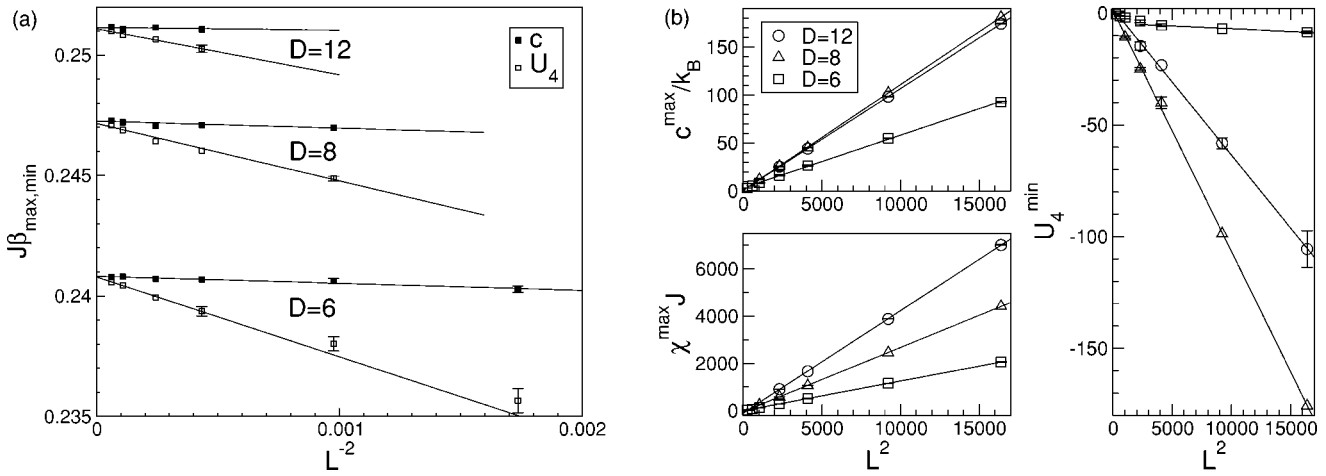

FIG. 14. (a) Extrapolation of peak positions $\beta_{\max,\min}(D,L)$ of the specific heat $c^{\max}$ and the fourth-order cumulant $U_4^{\min}$ for the different film thicknesses D. (b) Maxima of specific heat $c^{\max}$ and susceptibility $\chi^{\max}$, as well as minimum of the fourth-order cumulant $U_4^{\min}$ as functions of L^2.

$$\langle e^n\rangle = \frac{\int de' e'^n P_{L,D}(e')}{\int de' P_{L,D}(e')}. \tag{28}$$

Computing then $\langle e\rangle$ at the transition point by means of Eq. (28) we obtain

$$\langle e\rangle = \frac{e^+ + qe^-}{1+q} \tag{29}$$

(horizontal lines in Fig. 9), which is exact, apart from exponential corrections due to mixed phase contributions which are neglected in the double Gaussian approximation. Upon using the fluctuation relation (15) or $c = d\langle e\rangle/dT$ in conjunction with Eq. (28) one can calculate the specific heat to leading order,

$$c = \frac{a^+c^+ + a^-c^-}{a^+ + a^-} + \frac{[e^+ - e^- + (c^+ - c^-)\Delta T]^2}{(a^+ + a^-)^2}\frac{a^+a^-}{k_B T^2}L^2 D, \tag{30}$$

which is seen to take its maximum for $a^+ = a^-$ in Eq. (25). The position of the latter is thereby shifted away from the infinite-lattice transition temperature by an amount of

$$\Delta T = T_{c^{\max}}(D,L) - T_{\rm tr}(D) = k_B T_{\rm tr}^2 \frac{\ln q}{\Delta e D}\frac{1}{L^2}, \tag{31}$$

and the height of the peak is found to be

$$c^{\max} = \frac{c^+ + c^-}{2} + \frac{\Delta e^2 D}{4k_B T_{\rm tr}^2}L^2, \tag{32}$$

where $\Delta e \equiv e^+ - e^-$ is the latent heat. For convenience we may reexpress Eq. (31) in terms of the inverse temperature $\beta = 1/k_B T$ which yields

$$\beta_{c^{\max}}(D,L) = \beta_{\rm tr}(D) - \frac{\ln 2}{\Delta e D}\frac{1}{L^2}. \tag{33}$$

Thus, the inverse temperature $\beta_{c^{\max}}(D)$ at which the specific heat peaks provides a definition for a finite-lattice (pseudo) transition temperature from which the infinite-lattice transition temperature can be estimated via finite size scaling, i.e., by extrapolating $L\to\infty$.

A similar argumentation applies to the distribution of the order parameter $P_{L,D}(m)$ [25] yielding the same scaling behavior for the susceptibility χ, i.e.,

$$\beta_{\chi^{\max}}(D,L) - \beta_{\rm tr}(D) \propto (L^2 D)^{-1}, \tag{34}$$

$$\chi^{\max} \propto L^2 D, \tag{35}$$

and one can show that the fourth order cumulant U_4 (Fig. 12) takes a minimum value at an inverse temperature $\beta_{U_4^{\min}}(D,L)$ which is again shifted

$$\beta_{U_4^{\min}}(D,L) - \beta_{\rm tr}(D) \propto (L^2 D)^{-1}, \tag{36}$$

while the minimum $U_4^{\min}$ obeys

$$U_4^{\min} \propto -L^2 D. \tag{37}$$

Furthermore it was shown [25] that the shift in the crossing points of the cumulants for different system sizes is proportional to N^{-2}, which is negligibly small on the scale of $N = L^2 D$. Figure 14(b) now shows the maximum values of the response functions $c^{\max}$,$\chi^{\max}$, and the minimum $U_4^{\min}$ of the cumulant as function of $1/L^2$ for the three different thicknesses $D=6,8,12$. As can be seen from the plots, the data comply well with the behavior predicted by expressions (32), (35), and (37). Considering the fourth-order cumulant U_4 in the case of $D=6$, one observes that subleading corrections to scaling are still present for the smaller linear dimensions L, but the expected linear behavior in L^2 is created for the three largest choices of L.

The definition for the finite-lattice transition temperature considered so far, e.g., Eq. (33), involves leading order cor-

TABLE II. Estimates for the latent heats $\Delta e(D)$ and the inverse transition temperatures of the first-order interface localization-delocalization transition for different film thicknesses D. $\beta_{c^{\max}}(D,\infty)$ and $\beta_{U_4^{\min}}(D,\infty)$ are the estimates of the transition point $\beta_{\rm tr}(D)$ originating from an extrapolation of peak positions as described in the text, while $\beta_{ew}(D,\infty)$ denotes the estimate from the equal weight rule (38). The final estimate of the inverse temperature $\beta_{\rm tr}(D)$ of the triple point is stated in the last column.

D	$\Delta e(D)/J$	$J\beta_{c^{\max}}(D)$	$J\beta_{U_4^{\min}}(D)$	$J\beta_{\rm ew}(D)$	$J\beta_{\rm tr}(D)$
6	0.261(6)	0.24082(2)	0.24079(4)	0.24082(1)	0.24082(4)
8	0.300(2)	0.24726(3)	0.24716(7)	0.24725(2)	0.24725(10)
12	0.236(3)	0.25115(4)	0.25109(4)	0.25117(2)	0.25115(10)

rections of $1/L^2$. An alternative definition of the transition temperature which has the additional benefit that the latter corrections are absent was given in Ref. [26]. Here, it is utilized that at the infinite-lattice transition point $\beta_{\rm tr}(D)$ all phases coexist, which implies that the sum of the weights of the q ordered phases equals q times the weight of the disordered phase, i.e.,

$$R(\beta_{\rm ew},L,D) \equiv \frac{\sum_{e\leqslant e_{\rm cut}} P_{L,D}(e,\beta_{\rm ew})}{\sum_{e>e_{\rm cut}} P_{L,D}(e,\beta_{\rm ew})} = q, \tag{38}$$

where $P_{L,D}(e)$ is the (finite-size) energy probability distribution, and $\beta_{\rm ew}(D,L)$ differs from $\beta_{\rm tr}(D)$ only by corrections exponentially small in system size. The energy $e_{\rm cut}$ appearing in Eq. (38) is taken to be the internal energy at the temperature where the specific heat is maximal [26].

C. Transition temperatures

Now, we can extract the infinite-volume transition point $\beta_{\rm tr}(D)$ from the finite-size data, i.e., as Eqs. (33) and (36) and suggests by fitting the peak positions for fixed D to

$$\beta_{\rm max,min}(D,L) = \beta_{\rm max,min}(D,\infty) + \frac{a}{L^2}, \tag{39}$$

where $\beta_{\rm max,min}(D,L)$ stands for the location of the maximum of the specific heat $\beta_{c^{\max}}(D,L)$ and the location of the minimum $\beta_{U_4^{\min}}(D,L)$ of the fourth-order cumulant at finite L, while $\beta_{\rm max,min}(D,\infty)$ denotes the infinite-volume limit ($L\to\infty$) of the corresponding inverse temperatures, which is an estimate of the infinite-system transition point $\beta_{\rm tr}(D)$. Alternatively, we have also employed the finite-volume estimator $\beta_{\rm ew}(D,L)$ of the transition point, as defined by the condition (38).

The individual results for the infinite-system transition points are summarized in Table II. In the last column of Table II we state our final estimate of the infinite-system transition point $\beta_{\rm tr}(D)$, based on weighted averages over the estimates listed in columns 2–4. Concerning the error in our final estimate of $\beta_{\rm tr}(D)$ we have also accounted for the scatter in the crossings of the energy curves as depicted in Fig. 9 and the crossings in the fourth-order cumulant U_4 (see Fig. 12). While we find that the order of magnitude of the error as determined from the various finite-lattice estimators considered above complies well with all the data for $D=6$, especially the latter crossing points, we may have uncontrolled errors in case of the larger thicknesses $D=8$ and 12, due to the aforementioned lack of statistics deep in the pure phases. In these cases we consider here as a conservative error estimate the extremal crossing points as an upper bound to the transition point, which results in the error of $\beta_{\rm tr}(D\geqslant 8)$ as given in the last column of Table II. Fitting the locations of the maxima of the specific heat to Eq. (39), as depicted in Fig. 14(a), one can also determine the latent heat Δe which is, however, less accurate than computing Δe from the distribution $P_{L,D}(E)$ via [27]

$$\Delta e(L,D) = \Delta e(D) + \text{const}\times L^{-2}, \tag{40}$$

which yields the values stated in column 2 of Table II. Concerning the extrapolation (39) of the positions of the minima $U_4^{\min}$ and the maxima $c^{\max}$ we have used only data for $L>32$ in the case of $D=6$. For these lattices, exponential corrections to $\beta_{\rm ew}(D,L)$ cannot be resolved within the achieved accuracy. This is also the case for the larger film thicknesses D and all choices of L. Hence, the values listed in Table II for $\beta_{\rm ew}(D)$ are simply averages over the various lateral system sizes L ($L>32$ in the case of $D=6$).

D. Wetting temperature of the semi-infinite system

In order to determine the wetting temperature $\beta_{\rm w}=\lim_{D\to\infty}\beta_{\rm tr}(D)$ of the semi-infinite system, we have studied Hamiltonian (1) with $D=12$ and $L=48$ along the branch of positive bulk magnetization at the inverse temperature $\beta=0.251$ near the expected location of the wetting temperature $\beta_{\rm w}(H_1)$. We have performed simulations for five different sets of surface fields (symmetric, i.e., $H_1=H_D$), namely, $H_1/J=-0.25$, -0.125, 0, 0.125, and 0.25, utilizing a conventional Metropolis algorithm in order to measure the surface magnetization $\langle m_1\rangle=\langle\Sigma_{i\in\text{surface }1}S_i\rangle/N$ using up to 10^7 MCS for averaging. This selection of surface fields allows one to reweight all fields in the range $[-0.25J,0.25J]$ for a range of inverse temperatures $J\beta\in[0.249,0.253]$. Note that the metastability is strong enough (cf. Fig. 3) that the system remains in the ordered phase (initially all spins up) even for $H_1/J=-0.25$. According to the Young equation [29] the walls are wetted by spin down, if the difference $\Delta\sigma_{\rm w}$ between the surface free energy of the wall with respect to a positively magnetized bulk $\sigma_{\rm w+}$ and the surface free energy against a negatively magnetized bulk $\sigma_{\rm w-}$ exceeds the interfacial tension σ of the 3D Ising model [28] at an infinite distance from the wall,

$$\Delta\sigma_{\rm w} = \sigma_{\rm w+} - \sigma_{\rm w-} > \sigma. \tag{41}$$

By symmetry $\sigma_{\rm w-}(-H_1)$ equals $\sigma_{\rm w+}(H_1)$, i.e., the free energy cost of a wall favoring spin up with respect to a positively magnetized bulk. Thus we can perform a thermodynamic integration [30]

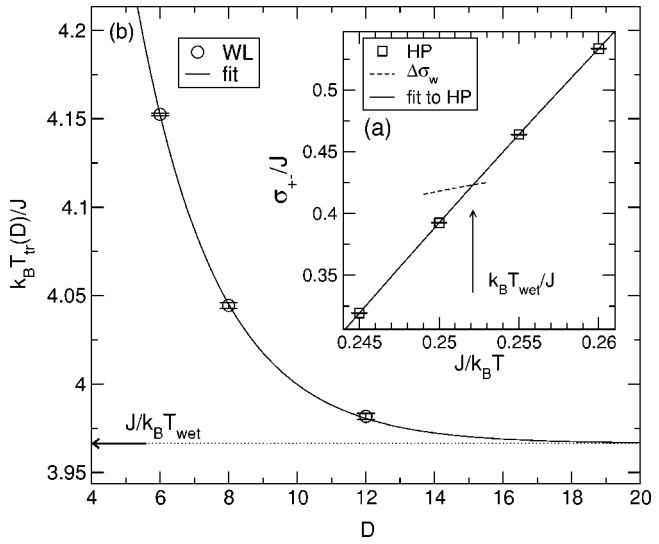

FIG. 15. (a) Shown are the interfacial tension σ of the 3D Ising model [Hasenbusch-Pinn (HP)] taken from Ref. [28], fitted by an eight-degree polynomial in order to smoothly interpolate between the data points as well as the the quantity $\Delta\sigma_w$ appearing in the Young equation (41). The position of the crossing point yields the wetting temperature $J\beta_w(H_1)=J/k_BT_w(H_1)=0.252\,12(5)$. (b) Transition temperatures, T_{tr}, as a function of film thickness, D, and fit to the expected exponential dependence.

$$\Delta\sigma_w = \sigma_{w+}(-H_1) - \sigma_{w+}(H_1) = \int_{-H_1}^{H_1} dH_1' \langle m_1(H_1')\rangle_\beta,$$

$$H_1 = 0.25J, \tag{42}$$

and determine the wetting temperature $\beta_w(H_1)$ by the condition $\Delta\sigma_w=\sigma$, which yields $J\beta_w(H_1)=0.252\,12(5)$ as depicted in Fig. 15(a).

Describing the semi-infinite system by means of the wetting film thickness l leads to the effective interface potential [5]

$$V_{eff}(l) = a\exp(-\kappa l) - b\exp(-2\kappa l) + c\exp(-3\kappa l), \tag{43}$$

which has the meaning of a free energy cost when placing a (flat) interface at distance l from the wall. Upon minimizing $V_{eff}(l)$ with respect to l one finds the equilibrium position of the interface. Equation (43) includes only the lowest powers of $\exp(-\kappa l)$ which are necessary to describe a first-order wetting transition in the semi-infinite system. The coefficient a explicitly depends on temperature, while the temperature dependence of b and c is neglected ($c>0$ in the following). [2] All coefficients have the same magnitude as the interfacial tension between bulk phases and one finds a first order wetting transition for $b>0$ at $a_w=b^2/4c$, where the interface jumps discontinuously into the bulk [9,31]. Now, for a film one has an additional contribution from the second wall and the effective potential reads [32]

$$\Delta V_{eff,film}(l) = V_{eff}(l) + V_{eff}(D-l) - 2V_{eff}(D/2)$$
$$= c[\tilde{m}^2(\tilde{m}^2 - r)^2 + t\tilde{m}^2], \tag{44}$$

with

$$r = \frac{b - 6c\,\exp(-\kappa D/2)}{2c} \tag{45}$$

and

$$t = \frac{a - a_w - b\,\exp(-\kappa D/2)}{c}. \tag{46}$$

In Eq. (44) we have utilized the auxiliary variable

$$\tilde{m} = 2\exp(-\kappa D/2)\{\cosh[\kappa(l - D/2)] - 1\}$$
$$= (\exp(-\kappa D/4)\kappa[l - D/2])^2 + [\text{higher orders of } (l - D/2)]. \tag{47}$$

In the film, $r>0$ gives rise to first-order interface localization-delocalization transitions and $t=0$ then denotes the triple temperature. Hence, for large D we have from Eq. (46)

$$a_{tr} = a_{wet} + b\exp(-\kappa D/2), \tag{48}$$

i.e., the triple temperature differs from the wetting temperature only by a term exponentially small in $\kappa D/2$ and is larger than the wetting temperature ($b>0$). Within mean field theory κ would have to be identified with the inverse bulk correlation length ξ_b [5]. However, from the two-field Hamiltonian approach developed in Ref. [33] we know that $\kappa/2$ has to be replaced by

$$\frac{\kappa}{2} = \frac{1}{2\xi_b\theta}, \quad \theta = 1 + \omega_{eff}/2, \tag{49}$$

where ω_{eff} is the effective wetting parameter which becomes $\lim_{T\to T_w^+}\omega_{eff}=k_BT/4\pi\sigma\xi_b^2$ upon lowering the temperature T toward the wetting temperature T_w [34]. From a simple exponential fit of the form (48) we get $\kappa/2=0.430(8)$. [Note that this has to be regarded as an effective value since we neglect any temperature dependence of κ within our range of triple temperatures $\beta_{tr}(D)$]. Evaluating now θ at $T_w/T_{cb}=0.88$ where we employ $\xi_b\sim 0.88$ [28] yields $\theta\sim 1.3$, which is compatible with the values extracted for θ by Parry *et al.* [34] and clearly differs from the value $\theta=1$ expected from mean field theory. Of course, making more quantitative statements would require data from additional film thicknesses D, but the above considerations clearly indicate that our data nicely support the asserted functional dependence of $\beta_{tr}(D)$ on D, i.e., Eq. (48).

IV. CONCLUSION

We have studied the interface localization-delocalization transition in a thin Ising film (1) for a choice of parameters,

[2] The description of the interface in terms of the effective interface potential V_{eff} follows from the sharp-kink approximation to the capillary wave Hamiltonian $\mathcal{H}_{eff}=\int d\rho[(\sigma/2)(\nabla l)^2+V_{eff}\{l(\rho)\}]$ where fluctuations of the local interface position are neglected.

where the transition is pronounced first order for all studied thicknesses $D=6$, 8, and 12. Checking for the correct behavior of the logarithm of the partition function $\ln Z$ which should converge to $N \ln 2$ as $\beta \to 0$, we find reasonable agreement for $D=6$ within error bars (cf. Table I). In contrast, for $D>6$ we see rather clear deviations from the expected value with relative deviations up to 10^{-3}. We attribute this behavior to a slowing down encountered in the flat energy-histogram ensemble. Difficulties also arise, when one considers to sample a flat magnetization distribution, although simulation results suggest that the slowing down is less severe. Here, we find evidence for a discontinuous shape transition, as studied by Neuhaus and Hager [18]. For the larger thicknesses ($D>6$) we therefore suggest employing an additional reference for the disordered phase (total number of states), in order to get the proper relative weight between the coexisting phases, thus correcting for the lack of tunneling events, in the late stages of the algorithm. The triple temperatures $\beta_{\mathrm{tr}}(D)$ of the interface localization delocalization transition can then be determined with a relative accuracy of the order 10^{-4} while the relative error in the latent heats is of the order 10^{-2}. The triple temperatures are seen to differ from the wetting temperature of the semi-infinite system by a term exponentially small in film thickness D as predicted by the sharp-kink approximation to the capillary wave Hamiltonian, provided the length scale κ is identified with the results of Parry and co-workers, i.e., Eq. (49).

When one compares the present results based on Wang-Landau sampling [13–16] to the first study of first-order interface localization-delocalization transitions [8] where simple Metropolis and heat-bath Monte Carlo algorithms were used, a major improvement of accuracy is clearly seen. On the other hand, the systematic problems due to entropic barriers described in our work show that it would be problematic to apply the Wang-Landau algorithm to larger systems than used here. Note that the largest sizes used by us, $128 \times 128 \times 12 \sim 1.97 \times 10^5$ Ising spins, distinctly exceed the sizes analyzed in most previous applications of this algorithm [13–16].

ACKNOWLEDGMENTS

This work was supported in part by the Deutsche Forschungsgemeinschaft under Grants No. Bi314/17. Helpful and stimulating discussions with D. P. Landau and P. Virnau are gratefully acknowledged. We thank the NICTR6/A5 Jülich and the HLR Stuttgart for a grant of computer time.

[1] A. O. Parry and R. Evans, Phys. Rev. Lett. **64**, 439 (1990).
[2] M. R. Swift, A. L. Owczarek, and J. O. Indekeu, Europhys. Lett. **14**, 475 (1991).
[3] J. O. Indekeu, A. L. Owczarek, and M. R. Swift, Phys. Rev. Lett. **66**, 2174 (1991).
[4] A. O. Parry and R. Evans, Phys. Rev. Lett. **66**, 2175 (1991).
[5] A. O. Parry and R. Evans, Physica A **181**, 250 (1992).
[6] K. Binder, D. P. Landau, and A. M. Ferrenberg, Phys. Rev. Lett. **74**, 298 (1995).
[7] K. Binder, D. P. Landau, and A. M. Ferrenberg, Phys. Rev. E **51**, 2823 (1995).
[8] A. M. Ferrenberg, D. P. Landau, and K. Binder, Phys. Rev. E **58**, 3353 (1998).
[9] M. Müller, E. V. Albano, and K. Binder, Phys. Rev. E **62**, 5281 (2000).
[10] M. Hasenbusch and K. Pinn, J. Phys. A **30**, 63 (1997).
[11] K. Binder, Z. Phys. B: Condens. Matter **45**, 61 (1981).
[12] R. Liebmann, Z. Phys. B: Condens. Matter **45**, 243 (1982).
[13] F. Wang and D. P. Landau, Phys. Rev. Lett. **86**, 2050 (2001).
[14] F. Wang and D. P. Landau, Phys. Rev. E **64**, 056101 (2001).
[15] B. J. Schulz, K. Binder, M. Müller, and D. P. Landau, Phys. Rev. E **67**, 067102 (2003).
[16] B. J. Schulz, K. Binder, and M. Müller, Int. J. Mod. Phys. C **13**, 477 (2002).
[17] A. B. Bortz, M. H. Kalos, and J. L. Lebowitz, J. Comput. Phys. **17**, 10 (1975).
[18] T. Neuhaus and S. Hager, J. Stat. Phys. **113**, 47 (2003).
[19] B. A. Berg, U. Hansmann, and T. Neuhaus, Phys. Rev. B **47**, 497 (1993).
[20] K.-T. Leung and R. K. P. Zia, J. Phys. A **23**, 4593 (1990).
[21] C. Borgs, R. Kotecky, and S. Miracle-Sole, J. Stat. Phys. **62**, 529 (1991).
[22] M. S. S. Challa, D. P. Landau, and K. Binder, Phys. Rev. B **34**, 1841 (1986).
[23] C. Borgs and K. Kotecky, J. Stat. Phys. **61**, 79 (1990).
[24] C. Borgs and J. Z. Imbrie, Commun. Math. Phys. **123**, 305 (1989).
[25] K. Vollmayt, J. D. Reger, M. Scheucher, and K. Binder, Z. Phys. B: Condens. Matter **91**, 113 (1993).
[26] C. Borgs and W. Janke, Phys. Rev. Lett. **68**, 1738 (1992).
[27] A. Billoire, T. Neuhaus, and B. Berg, Nucl. Phys. B **413**, 795 (1994).
[28] M. Hasenbusch and K. Pinn, Physica A **203**, 189 (1994).
[29] T. Young, Philos. Trans. R. Soc. London **5**, 65 (1805).
[30] M. Müller and K. Binder, Macromolecules **31**, 8323 (1998).
[31] M. Müller, K. Binder, and E. V. Albano, Physica A **279**, 188 (2000).
[32] M. Müller and K. Binder, Phys. Rev. E **63**, 021602 (2001).
[33] A. O. Parry and C. J. Boulter, Physica A **218**, 109 (1995).
[34] A. O. Parry, C. J. Boulter, and P. S. Swain, Phys. Rev. E **52**, R5768 (1995).
[35] S. Trebst, D. A. Huse, and M. Troyer, e-print cond-mat/0401195.